Electrically Driven Tuning of the Dielectric Constant in MoS_2 Layers

Elton J. G. Santos[†,§,*] and Efthimios Kaxiras[†,‡]

[†]School of Engineering and Applied Sciences, Harvard University, Cambridge, Massachusetts 02138, United States and [‡]Department of Physics, Harvard University, Cambridge, Massachusetts 02138, United States. [§]Present address: Department of Chemical Engineering, Stanford University, Stanford, California 94305, United States, and SUNCAT Center for Interface Science and Catalysis, SLAC National Accelerator Laboratory, Menlo Park, California 94025, United States

ABSTRACT The properties of two-dimensional materials, such as molybdenum disulfide, will play an important role in the design of the next generation of electronic devices. Many of those properties are determined by the dielectric constant which is one of the fundamental quantities used to characterize conductivity, refractive index, charge screening, and capacitance. We predict that the effective dielectric constant (ε) of few-layer MoS_2 is tunable by an external electric field (E_{ext}). Through first-principles electronic structure calculations, including van der Waals interactions, we show that at low fields (E_{ext} < 0.01 V/Å) ε assumes a nearly constant value ~4 but increases at higher fields to values that depend on the layer thickness. The thicker the structure, the stronger the modulation of ε with the electric field. Increasing of the external field perpendicular to the dichalcogenide layers beyond a critical value can drive the system to an unstable state where the layers are weakly coupled and can be easily separated. The observed dependence of ε on the external field is due to charge polarization driven by the bias. Implications on the optical properties as well as on the electronic excitations are also considered. Our results point to a promising way of understanding and controlling the screening properties of MoS_2 through external electric fields.

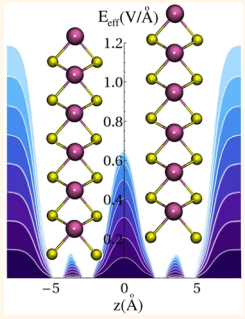

KEYWORDS: MoS_2 dielectric constant · dielectric response · tunable dielectric properties · electrostatic exfoliation · excitations

Layered molybdenum disulfide has been attracting increasing interest as a building block of a new class of nanodevices. MoS_2 offers a novel set of features, for example, as an alternative 2D material that overcomes the limitation of a zero band gap in graphene. The sizable band gap observed in monolayer MoS_2[1] has opened new avenues for the creation of field-effect transistors with power dissipation lower than conventional transistors,[2,3] optoelectronics devices in high-performance flexible electronics,[4] and thin-film solar cells[5−7] that can absorb light in the visible range.[8] One of the main features that influences all these properties is the MoS_2 thickness, which determines the charge distribution in the device as well as the electronic structure through the band gap and the electric field screening that depends on the dielectric constant ε. The large range of values for ε found by different experiments[9−13] (from 4 to 17) has become a subject of considerable discussion. As is also the case in graphene,[14] the presence of substrates plays a role in the experimental attempts to measure the intrinsic dielectric constant in MoS_2 layers. In particular, recent electrical transport measurements[15] have shown that the dielectric response of MoS_2 layers is sensitive to the substrate used and the effect depends on the sample thickness. In practical terms, the effective dielectric constant of a two-dimensional crystal is given by $\varepsilon = (\varepsilon_{sub} + \varepsilon_{vac})/2$, with ε_{sub} and ε_{vac} being the dielectric constant values for the underlying substrate and vacuum, respectively. However, using this approach requires detailed knowledge of the dielectric constant of the environment in which MoS_2 is embedded, which is not always accessible. The determination of the intrinsic value of ε is thus of great interest and importance as it can lead to novel routes for improving the performance of MoS_2-based devices and reveal the role of electric-field screening in van der Waals layered structures.

Here we show that ε can be manipulated by an external electric field E_{ext}, with resulting values in the range of 4−16. Bilayer (2L) MoS_2 does not show substantial modifications with the external field, while *N*-layer MoS_2 ($N > 2$) displays a dependence of ε on the external bias. The linear response of the

* Address correspondence to eltonjos@stanford.edu.

Received for review July 19, 2013 and accepted November 11, 2013.

Published online November 11, 2013
10.1021/nn403738b

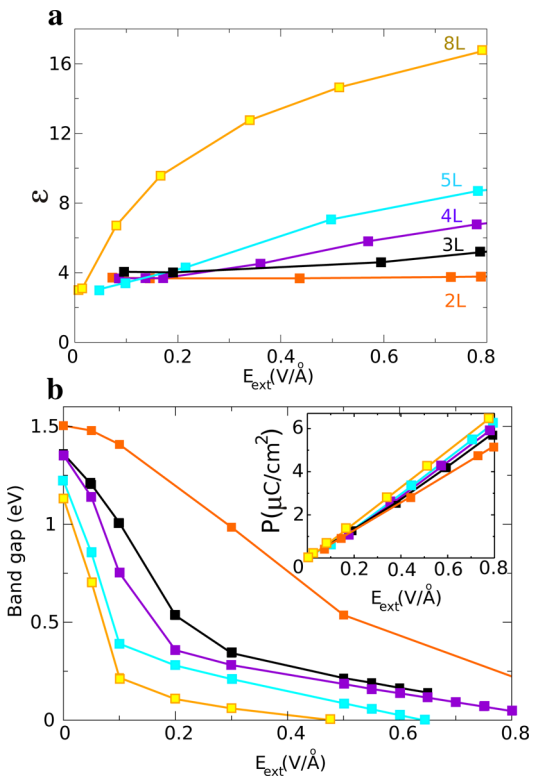

Figure 1. (a) Calculated dielectric constant ε as a function of E_{ext} (V/Å) for 2L−8L MoS_2. The AB stacking was used for all calculations. (b) Band gap (eV) and polarization P (μC/cm^2) (inset) as a function of E_{ext} using the same labeling scheme for the MoS_2 layers as in a.

polarization of MoS_2 as a function of the electric field is the main driving force of the tuning, with the electric field being partially screened by thinner MoS_2 crystals similar to the behavior observed in graphene structures.[16] The interlayer coupling is also modified with the electric bias, which produces two effects: a new set of excitations inside the band gap and a transition from semiconducting to metallic behavior, and a decreasing of the van der Waals energy barrier that keeps the layers bound. This suggests the possibility of layer exfoliation through an electrostatic gate.

RESULTS

Figure 1a displays how ε evolves with external fields for different number of MoS_2 layers. At low fields, $E_{ext} \leq$ 0.001 V/Å, ε is almost independent of the number of layers having a value close to ∼4. As the external field E_{ext} is increased, ε reaches larger values, up to ε = 16.8 at E_{ext} =0.8 V/Å for N = 8 layers with a roughly linear dependence of ε on the number of layers N at a fixed value of the field. These values for ε agree well with those found by theoretical groups.[17−19] The electric susceptibility χ (not shown) extracted from the polarization P clearly shows the roughly linear dependence on the number of layers N. This is in close agreement with electrical transport measurements[20] performed on MoS_2 field-effect transistors as a function of thickness. We note that electric fields of the magnitude considered here can in principle be achieved and controlled, as reported, for instance, recently in the case of trilayer graphene,[21] where fields as high as 0.6 V/Å were attained using top and bottom HfO_2 gates. Moreover, the high electric breakdown of MoS_2 layers allows the application of large electric bias as recently measured by Lembke *et al.*[22]

The behavior of the band gap as a function of applied external field is also shown in Figure 1b and is a monotonically but not uniformly decreasing function of the field. This clearly demonstrates the dramatic effect that the external field has on the electronic structure (this is further analyzed later). The polarization P also exhibits a strong dependence on the applied field (see inset in Figure 1b). The change in P with the layer thickness N is weaker than that of the dielectric function or the band gap, which can be explained by the fact that the polarization is given by $P = \chi E_{eff}$, where χ is the electric susceptibility, related to the dielectric constant by $\chi = (\varepsilon - 1)/4\pi$, and E_{eff} is the effective field within the material; E_{eff} decreases with the number of layers N as discussed in more detail later, while χ increases with N, as Figure 1a shows, leading to a weaker dependence of P on N.

The origin of the electric-field-mediated tunable dielectric constant in MoS_2 layered systems is shown in Figure 2. We focus on the response of 2L MoS_2 that captures the essential features. The application of E_{ext} generates an interlayer charge transfer which partially cancels the external field, producing an effective field E_{eff} in the region between the layers. At low E_{ext}, all values of E_{eff} are approximately constant (within the numerical accuracy of our model). At fields close to those used in MoS_2 transistors,[2] 0.08 V/Å, E_{eff} is already dependent on position, with the maximum value in the region between the layers occurring at the midpoint between the layers, similar to what is observed for multilayer graphene.[23] The induced charge densities, $\Delta\rho$, at different fields (Figure 2b) show a charge accumulation at the layer that is under positive potential and a corresponding depletion at the other one. The integration of $\Delta\rho$ along the direction perpendicular to the layers (z coordinate), using the Poisson equation $\nabla^2 V(z) = -\Delta\rho/\varepsilon_0$, where ε_0 is the vacuum permittivity, results in a response electric field E_ρ (dashed line in Figure 2b) that screens the external electric field, that is, $E_{eff} \approx E_{ext} - E_\rho$.

We address next the dependence of ε on the number of MoS_2 layers N. In Figure 3, we show E_{eff} as a function of the position z for N = 2, 3, 5. The application of E_{ext} on thicker MoS_2 structures generates a lower E_{eff} inside the slab. For instance, in the N = 5 case, the maximum value of E_{eff} between the two MoS_2 layers is ∼3 times smaller than that between the layers in the N = 2 system. As ε is determined by the ratio of the external and internal fields, the enhancement in

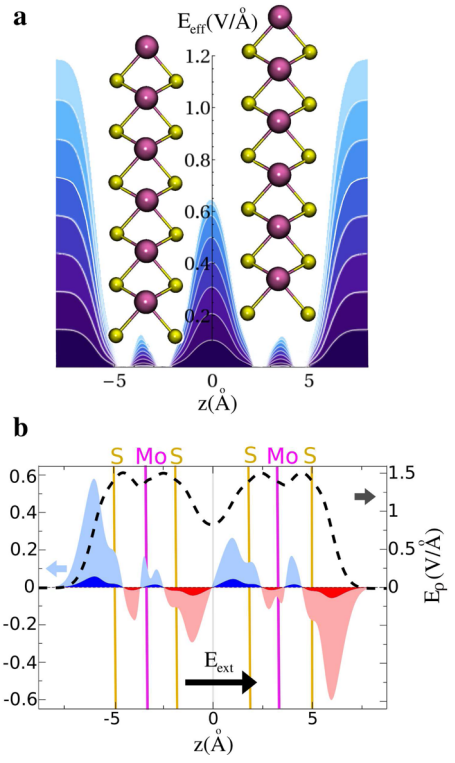

Figure 2. (a) Effective electric field, E_{eff}, as a function of the interlayer distance at different external fields E_{ext} for bilayer MoS_2. (b) Induced charge densities, $\Delta\rho = \rho(E_{ext}) - \rho(0)$, in e/Å^3, between the two MoS_2 planes. The bolder and lighter shaded curves correspond to E_{ext} = 0.14 V/Å and E_{ext} = 1.5 V/Å, respectively. The dashed line curve corresponds to the electric field generated by the induced charge (E_ρ) at E_{ext} = 1.5 V/Å. The large black arrow shows the direction of E_{ext} relative to the bilayer structure. The positions of S and Mo atoms are marked by the colored (yellow for S, purple for Mo) vertical lines.

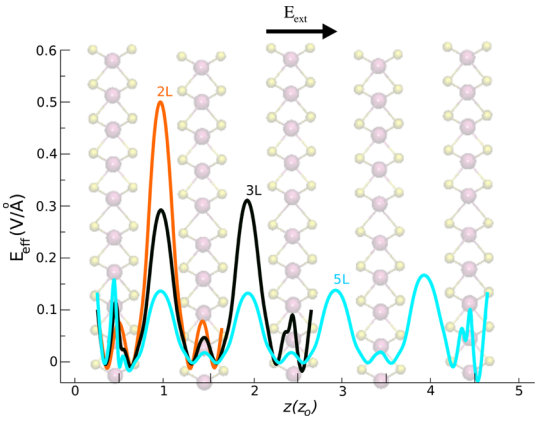

Figure 3. E_{eff} as a function of the interlayer position (z_0 = 6.70 Å) for 2L (red), 3L (green), and 5L (blue) MoS_2 (the dichalcogenide layers are shown in the background). The black arrow indicates the orientation of E_{ext}. The applied field is 0.73 V/Å.

the value of the dielectric constant with the number of layers N is directly related to the reduction of the field in the innermost regions of the structure which leads to lower ε values for lower values of N. This decay of field with the thickness of MoS_2 layers is in good agreement with recent electrostatic force microscopy[24] and Kelvin probe microscope[25] measurements.

The interplay of electric fields and the MoS_2 thickness also influences other properties, for instance, the optical conductivity σ. Figure 4 shows the in-plane (solid line) and the out-of-plane (dashed line) conductivity (in $10^3\ \Omega^{-1}\ m^{-1}$) as a function of the frequency ω (in eV) for 2L, 5L, and 9L structures. Both conductivities are defined in relation to the polarization vector being perpendicular (in-plane) and parallel (out-of-plane) to the z axis. Excitonic effects are not taken into account here; that is, we are confining the discussion of the electrical and optical response to a *noninteracting* picture. Many-body effects, such as electron−electron and electron−hole interactions, as well as local field effects should be included in a full description of the properties. At E_{ext} = 0.0 V/Å, the out-of-plane optical response is mainly confined to energies higher than 2 eV (Figure 4a, $e_{\Gamma-\Gamma}$ excitations) that systematically decreases to lower values as the number of layers increases. This can be understood in terms of the electronic band structure of the structures with different number of layers (Figure 4b), which shows that, as the MoS_2 thickness increases, the energy difference between the top and bottom of the valence and conduction bands, respectively, decreases at Γ, which determines the optical response for this polarization. This behavior is in agreement with photoluminescence measurements which show that thicker MoS_2 structures have smaller band gaps.[1] As the polarization is in-plane (Figure 4a), lower excitation energies (e_{K-K}) appear which occur at the K-point, as shown in Figure 4b. The different number of layers slightly shifts the position of the e_{K-K} transitions to lower frequencies and enhances their signal with increasing N at higher energies. Indeed, in the spectral range of 1.7−2.0 eV, there exist two optical transitions labeled A and B[12] that are directly associated with the excitonic character of the emission peaks, which are not resolved here due to the omission of spin−orbit coupling and many-body effects as discussed above.[13] Nevertheless, the in-plane optical conductivity (Figure 4a) shows that such features exist even in the noninteracting picture. In addition, we note that the position of the top of the valence band (VB) and the bottom of the conduction band (CB) in the band structure of MoS_2 structures is sensitive to some details in the calculation such as the interlayer lattice distance, exchange-correlation functional, and reciprocal-space grid point sampling utilized. The differences in their values due to different choices of computational parameters can be as high as 67 meV, which can change the position of CB or VB in the Brillouin zone. We obtained well-converged values that avoid these pitfalls through a systematic convergence study.

For $E_{ext} > 0$, the electric bias induces modifications on the out-of-plane optical conductivity with

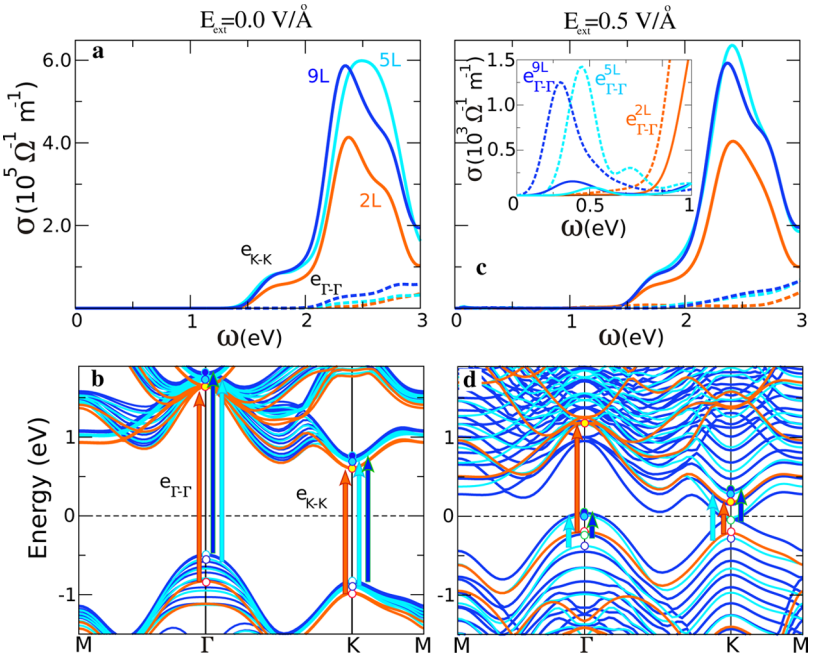

Figure 4. (a) Optical conductivity σ ($10^3\ \Omega^{-1}\ m^{-1}$) as a function of the frequency ω (eV) of 2L (orange), 5L (light blue), and 9L (dark blue) MoS_2 at E_{ext} = 0.0 V/Å. The in-plane and out-of-plane components are shown by solid and dashed lines, respectively, for each stacking. (b) Electronic band structures for 2L, 5L, and 9L MoS_2 at E_{ext} = 0.0 V/Å with the same labels as in a. The dashed line shows E_F which is set to 0. The allowed interband transitions at K, e_{K-K}, and Γ, $e_{\Gamma-\Gamma}$, are marked by arrows with the resulting peaks at energies shown in a. (c,d) Similar to a and b, respectively, but at E_{ext} = 0.5 V/Å. The biased electronic transitions at Γ are shown for each stacking as $e^n_{\Gamma-\Gamma}$ (n = 2L, 5L, 9L), in the inset in c, with the electronic levels involved in d. The electronic transitions at K are also marked, but they have smaller intensity compared to those at Γ.

the appearance of peaks in the infrared (0.20−1.18 eV), as shown in the inset in Figure 4c. These peaks, labeled $e^{NL}_{\Gamma-\Gamma}$ (N = 2, 5, 9), originate from the interband transitions at the Γ-point between states close to the Fermi level (E_F) for each stacking. Figure 4d shows the corresponding excitations marked by arrows. The $e_{\Gamma-\Gamma}$ transitions are mainly of p−d character between the band edges for 2L, 5L, and 9L MoS_2.[13] For the case of in-plane polarization, the external electric field induces small variations of the optical conductivity at lower frequencies (inset in Figure 4c). The relatively weaker in-plane optical response is due to the different amount of p and d states at K which diminishes the intensity of the peaks.[26] At energies higher than 1.6 eV, the in-plane response shows little modification for the structures with different number of layers, with slight variations on the peak shape. This behavior is in agreement with recent optical absorption experiments, performed on few-layer MoS_2 in a field-effect transistor geometry.[27]

Finally, we find that there is a limit on the magnitude of E_{ext} that can be applied to the system. Figure 5 shows the total energy for bilayer MoS_2 as a function of the interlayer distance z. For E_{ext} = 0.0 V/Å, a van der Waals barrier (E_{vdW}) of 30 meV/atom prevents the separation of the two layers from z_0 to infinity. For $E_{ext} \neq 0$, the value of E_{vdW} decreases, indicating that the MoS_2 layers become less bound. At E_{ext} = 2.0 V/Å, the two dichalcogenide layers can be easily separated with a barrier of only 0.45 meV/atom. This suggests that an

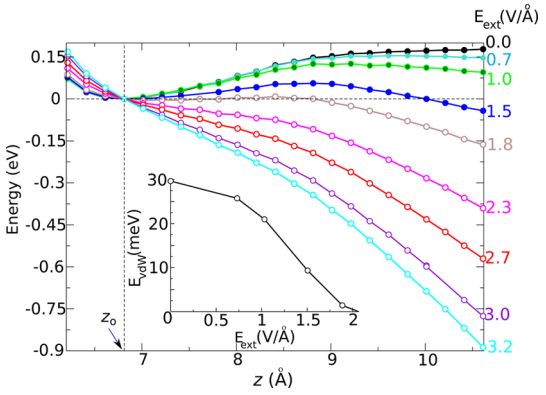

Figure 5. Energy per unit cell *versus* interlayer distance for different values of E_{ext} in V/Å. The vertical dashed line indicates the equilibrium interlayer distance z_0 = 6.70 Å. The inset shows the van der Waals barrier (E_{vdW}) per atom as a function of E_{ext}.

electrostatic gate can be used to exfoliate dichalcogenide layered materials as an alternative to chemical[28] or mechanical exfoliation.[1] The existence of an electrostatic field that can be used to exfoliate layered materials was successfully applied to graphene, in which case highly oriented pyrolytic graphite has been exfoliated to produce prepatterned few-layer graphene.[29]

CONCLUSIONS

We have considered the interplay between electric fields and screening properties of few-layer molybdenum

disulfide, which is an interesting material for future applications in electronic and optoelectronic devices. We find that the effective dielectric constant is electrically tunable, with the MoS_2 thickness playing an important role in the enhancement of the tuning. The thicker the MoS_2 structure is, the stronger the tuning with electric bias. The driving force for such behavior is due to the linear dependence of the electrical polarization of MoS_2 on the external field. The response field calculated from the polarization charge does not screen completely the external electric bias. The optical conductivity is used to study the excitations in both in-plane and out-of-plane polarizations. In finite fields, prominent peaks exist inside the original band gap (infrared range) which are generated due to interband transitions at lower energies. The existence and intensity of these features depend on the MoS_2 thickness and on the field strength. The induced interlayer charge imbalance generated by the bias can also drive the system to an unstable state where the layers can be separated from each other, suggesting an electrostatic exfoliation process.

The behavior reported here for MoS_2 is likely to be obtained in other layered materials of similar structure, like the family of metal dichalcogenides MX_2 (M = W, Mo; X = Se, S, Te), which have semiconducting properties,[30] as well as in combinations of layered materials, for instance, the recently observed combination of graphene and MoS_2 layers in a vertical heterojunction device.[31] The dependence of the dielectric response of these structures on two easily accessible parameters, the thickness in terms of number of layers involved and the externally applied electric field, opens new possibilities in the design of interesting devices with tunable response and possibly new physics of the confined and driven electronic states.

METHODS

The simulations reported here are based on density functional theory calculations using the SIESTA code.[32] We have used the nonlocal van der Waals density functional for the exchange-correlation term.[33] We used a double-ζ polarized basis and norm-conserving Troullier−Martins pseudopotentials.[34] Atomic coordinates were allowed to relax using a conjugate-gradient algorithm until all forces were smaller in magnitude than 0.01 eV/Å. Specifically, we included the relaxation of the out-of-plane distance between layers and the in-plane lattice constant at each value of the external electric field. To avoid interactions between layer images, the distance between periodic images of the MoS_2 structures along the direction perpendicular to the dichalcogenide plane was set larger than 20 Å. The resolution of the real-space grid used to calculate the Hartree and exchange-correlation contributions to the total energy was chosen to be equivalent to 150 Ry plane-wave cutoff. The number of k-points was chosen according to the Monkhorst−Pack[35] scheme and was set to the equivalent of a $44 \times 44 \times 1$ grid in the primitive unit cell of MoS_2, which gives well-converged values for all the calculated properties. We used a Fermi−Dirac distribution with an electronic temperature of $k_BT = 21$ meV.

We applied a spatially periodic sawtooth-like potential perpendicular to the MoS_2 layers which simulates the external field across the supercell. The MoS_2 layers exhibit no spontaneous polarization, which facilitates the description of the periodic boundary conditions under an applied electric field. The calculation of the dielectric constant is based on a formulation from ref 36. The polarization $P = \chi E_{\text{eff}}$ corresponds to an electric dipole moment of magnitude $m = PV = (\chi E_{\text{eff}})(dA)$, where d is the MoS_2 thickness, A is the cross section of the unit cell, and $V = Ad$ is the volume of the MoS_2 layer. The dipole moment density is given by $(m/A) = \chi E_{\text{eff}} d$, which gives rise to an electrostatic potential ΔV in MoS_2: $\Delta V = 4\pi(m/A) = 4\pi\chi E_{\text{eff}} d$. The SIESTA code works with periodic boundary conditions (PBC) and includes automatically a compensating field, $E_{\text{PBC}} = \Delta V/c$, to cancel this electrostatic potential shift along the total length c of the supercell in the same direction as the applied field. This compensating field is added to the input field E_{inp} in the calculation which results in a field E_{ext} outside of the MoS_2 layers of intensity

$$E_{\text{ext}} = E_{\text{inp}} + E_{\text{PBC}} = E_{\text{inp}} + \frac{4\pi\chi E_{\text{eff}} d}{c}$$

Assuming that the normal component of the electric displacement D is conserved gives $E_{\text{ext}} = D = E_{\text{eff}} + 4\pi P = E_{\text{eff}}(1 + 4\pi\chi)$ from which we obtain

$$\chi = \frac{1}{4\pi} \frac{E_{\text{inp}} - E_{\text{ext}}}{E_{\text{ext}}(1 - d/c) - E_{\text{inp}}}$$

The value of ε can then be obtained by using $\varepsilon = 1 + 4\pi\chi$ with E_{inp} as the input value of the electric field in the calculation and E_{ext} as the calculated output field, after self-consistency, in the region far from the MoS_2 layers.

The values of the spatially varying effective electric field $E_{\text{ext}}(\mathbf{r})$ shown in Figure 2 were calculated taking a derivative with respect to the distance of the averaged electrostatic potential $\langle V_H(\mathbf{r})\rangle$ by finite differences between a calculation at 0 and at a finite value of the external field. $\langle V_H(\mathbf{r})\rangle$ was calculated by taking the planar average over planes parallel to the atomic planes, followed by a convolution with a filter function to eliminate oscillations and conserve only those features that are relevant on a macroscopic scale.[37] For the calculation of the value of ε, we have used the expression mentioned above in terms of χ that involves only the values of E_{ext} and E_{inp} and not $E_{\text{ext}}(\mathbf{r})$; this method avoids any dependence of ε on the filter functions that could give different numerical values depending on the length of the step function used.[37] Value of $\Delta\rho(\mathbf{r})$ was calculated using a similar procedure as that for $E_{\text{ext}}(\mathbf{r})$, taking the total charge density distribution (ionic plus electronic) as the initial quantity. The spatially varying polarization $\mathbf{P}(\mathbf{r})$ was calculated by the integration of $\Delta\rho(\mathbf{r})$ through $\nabla\cdot\mathbf{P}(\mathbf{r}) = -\Delta\rho(\mathbf{r})$ for each external field value.

The calculation of the optical properties was based on the computation of the complex dielectric function $\varepsilon(\omega) = \varepsilon_1(\omega) + i\varepsilon_2(\omega)$, in which the imaginary part $\varepsilon_2(\omega)$ is given by

$$\varepsilon_2(\omega) = \frac{e^2\hbar}{\pi m^2\omega^2} \sum_{i,j} \int_{\text{BZ}} d\mathbf{k} |W_{ij}(\mathbf{k})|^2 \delta[\omega - \omega_{ij}(\mathbf{k})] \qquad (1)$$

where the integral is over all $\mathbf{k}$-points in the Brillouin zone (BZ) and the sum runs over all possible pairs of valence $|\phi_i\rangle$ and conduction $|\phi_j\rangle$ bands with corresponding eigenvalues E_i and E_j, such that $\hbar\omega_{ij}(\mathbf{k}) = E_j - E_i$. The electric dipole transition matrix element $W_{ij}(\mathbf{k})$, which represents the transition rate of an electron from state $|\phi_i\rangle$ to state $|\phi_j\rangle$, is given by $W_{ij}(\mathbf{k}) = \langle\phi_j(\mathbf{k})|\hat{\mathbf{e}}\cdot\mathbf{p}|\phi_i(\mathbf{k})\rangle$, with $\hat{\mathbf{e}}$ and $\mathbf{p}$ being the polarization vector and the momentum operator, respectively. The optical conductivity is given by $\sigma(\omega) = (\omega/4\pi)(\varepsilon_2(\omega) - 1)$.[38] We found the dielectric function and optical conductivity to be sufficiently well-converged with a mesh of $30 \times 30 \times 1$ k-points. A Gaussian broadening of 100 meV was used to plot the optical conductivity as a function of the frequency.

Conflict of Interest: The authors declare no competing financial interest.

Acknowledgment. We have used computational resources provided by the Extreme Science and Engineering Discovery Environment (XSEDE), supported by NSF Grant Nos. TG-DMR-120073, TG-DMR120049, and TG-PHY120021.

REFERENCES AND NOTES

1. Mak, K. F.; Lee, C.; Hone, J.; Shan, J.; Heinz, T. F. Atomically Thin MoS_2: A New Direct-Gap Semiconductor. *Phys. Rev. Lett.* **2010**, *105*, 136805–136809.
2. Radisavljevic, B.; Radenovic, A.; Brivio, J.; Giacometti, V.; Kis, A. Single-Layer MoS_2 Transistors. *Nat. Nanotechnol.* **2011**, *6*, 147–150.
3. Yoon, Y.; Ganapathi, K.; Salahuddin, S. How Good Can Monolayer MoS_2 Transistors Be?. *Nano Lett.* **2011**, *11*, 3768–3773.
4. Bertolazzi, S.; Brivio, J.; Kis, A. Stretching and Breaking of Ultrathin MoS_2. *ACS Nano* **2011**, *5*, 9703–9709.
5. Shanmugam, M.; Bansal, T.; Durcan, C. A.; Yu, B. Molybdenum Disulphide/Titanium Dioxide Nanocomposite-Poly 3-Hexylthiophene Bulk Heterojunction Solar Cell. *Appl. Phys. Lett.* **2012**, *100*, 153901–153905.
6. Yin, Z.; Li, H.; Li, H.; Jiang, L.; Shi, Y.; Sun, Y.; Lu, G.; Zhang, Q.; Chen, X.; Zhang, H. Single-Layer MoS_2 Phototransistors. *ACS Nano* **2012**, *6*, 74–80.
7. Shanmugam, M.; Durcan, C. A.; Yu, B. Layered Semiconductor Molybdenum Disulfide Nanomembrane Based Schottky-Barrier Solar Cells. *Nanoscale* **2012**, *4*, 7399–7405.
8. Lee, H. S.; Min, S. W.; Chang, Y. G.; Park, M. K.; Nam, T.; Kim, H.; Kim, J. H.; Ryu, S.; Im, S. MoS_2 Nanosheet Phototransistors with Thickness-Modulated Optical Energy Gap. *Nano Lett.* **2012**, *12*, 3695–3700.
9. Zhang, X.; Hayward, D. O.; Mingos, D. M. P. Dielectric Properties of MoS_2 and Pt Catalysts: Effects of Temperature and Microwave Frequency. *Catal. Lett.* **2002**, *84*, 225–233.
10. Kim, S.; Konar, A.; Hwang, W. S.; Lee, J. H.; Lee, J.; Yang, J.; Jung, C.; Kim, H.; Yoo, J. B.; Choi, J. Y.; *et al.* High-Mobility and Low-Power Thin-Film Transistors Based on Multilayer MoS_2 Crystals. *Nat. Commun.* **2012**, *3*, 1011–1018.
11. Bell, M. G.; Liang, W. Y. Electron Energy Loss Studies in Solids: The Transition Metal Dichalcogenides. *Adv. Phys.* **1976**, *1976*, 53–86.
12. Frindt, R. F.; Yoffe, A. D. Physical Properties of Layer Structures: Optical Properties and Photoconductivity of Thin Crystals of Molybdenum Disulphide. *Proc. R. Soc. London, Ser. A* **1963**, *273*, 69–83.
13. Beal, A. R.; Hughes, H. P. Kramers−Kronig Analysis of the Reflectivity Spectra of 2H-MoS_2, 2H-$MoSe_2$ and 2H-$MoTe_2$. *J. Phys. C: Solid State Phys.* **1979**, *12*, 881–890.
14. Hwang, C.; Siegel, D. A.; Mo, S. K.; Regan, W.; Ismach, A.; Zhang, Y.; Zettl, A.; Lanzara, A. Fermi Velocity Engineering in Graphene by Substrate Modification. *Sci. Rep.* **2012**, *2*, 590.
15. Bao, W.; Cai, X.; Kim, D.; Sridhara, K.; Fuhrer, M. S. High Mobility Ambipolar MoS_2 Field-Effect Transistors: Substrate and Dielectric Effects. *Appl. Phys. Lett.* **2013**, *102*, 042104–042108.
16. Datta, S. S.; Strachan, D. R.; Mele, E. J.; Johnson, A. T. C. Surface Potentials and Layer Charge Distributions in Few-Layer Graphene Films. *Nano Lett.* **2009**, *9*, 7–11.
17. Reshak, A. H.; Auluck, S. Calculated Optical Properties of 2H−MoS_2 Intercalated with Lithium. *Phys. Rev. B* **2003**, *68*, 125101–125108.
18. Molina-Sánchez, A.; Wirtz, L. Phonons In Single-Layer and Few-Layer MoS_2 and WS_2. *Phys. Rev. B* **2011**, *84*, 155413–155421.
19. Cheiwchanchamnangij, T.; Lambrecht, W. R. L. Quasiparticle Band Structure Calculation of Monolayer, Bilayer, and Bulk MoS_2. *Phys. Rev. B* **2012**, *85*, 205302–205306.
20. Min, S.-W.; Lee, H. S.; Choi, H. J.; Park, M. K.; Nam, T.; Kim, H.; Ryu, S.; Im, S. Nanosheet Thickness-Modulated MoS_2 Dielectric Property Evidenced by Field-Effect Transistor Performance. *Nanoscale* **2013**, *5*, 548–551.
21. Zou, K.; Zhang, F.; Clapp, C.; MacDonald, A. H.; Zhu, J. Transport Studies of Dual-Gated ABC and ABA Trilayer Graphene: Band Gap Opening and Band Structure Tuning in Very Large Perpendicular Electric Fields. *Nano Lett.* **2013**, *13*, 369–373.
22. Lembke, D.; Kis, A. Breakdown of High-Performance Monolayer MoS_2 Transistors. *Nano Lett.* **2012**, *12*, 10070–10075.
23. Santos, E. J. G.; Kaxiras, E. Electric-Field Dependence of the Effective Dielectric Constant in Graphene. *Nano Lett.* **2013**, *13*, 898–902.
24. Castellanos-Gomez, A.; Cappelluti, E.; Roldán, R.; Agrait, N.; Guinea, F.; Rubio-Bollinger, G. Electric-Field Screening in Atomically Thin Layers of MoS_2: the Role of Interlayer Coupling. *Adv. Mater.* **2013**, *25*, 899–903.
25. Li, Y.; Xu, C.-Y.; Zhen, L. Surface Potential and Interlayer Screening Effects of Few-Layer MoS_2 Nanoflakes. *Appl. Phys. Lett.* **2013**, *102*, 143110–143114.
26. Bromley, R. A.; Murray, R. B.; Yoffee, A. D. The Band Structures of Some Transition Metal Dichalcogenides: III. Group VI A: Trigonal Prism Materials. *J. Phys. C: Solid State Phys.* **1972**, *5*, 759–778.
27. Newaz, A. K. M.; Prasai, D.; Ziegler, J. I.; Caudel, D.; Robinson, S.; Haglund, R. F., Jr.; Bolotin, K. I. Electrical Control of Optical Properties of Monolayer MoS_2. *Solid State Commun.* **2013**, *155*, 49–52.
28. Coleman, J. N.; Lotya, M.; O'Neill, A.; Bergin, S. D.; King, P. J.; Khan, U.; Young, K.; Gaucher, A.; De, S.; Smith, R. J.; *et al.* Two-Dimensional Nanosheets Produced by Liquid Exfoliation of Layered Materials. *Science* **2011**, *331*, 568–571.
29. Liang, X.; Chang, A. S. P.; Zhang, Y.; Harteneck, B. D.; Choo, H.; Olynick, D. L.; Cabrini, S. Electrostatic Force Assisted Exfoliation of Prepatterned Few-Layer Graphenes into Device Sites. *Nano Lett.* **2009**, *9*, 467–472.
30. Wang, Q. H.; Kalantar-Zadeh, K.; Kis, A.; Coleman, J. N.; Strano, M. S. Electronics and Optoelectronics of Two-Dimensional Transition Metal Dichalcogenides. *Nat. Nanotechnol.* **2012**, *7*, 699–712.
31. Britnell, L.; Gorbachev, R. V.; Jalil, R.; Belle, B. D.; Schedin, F.; Mishchenko, A.; Georgiou, T.; Katsnelson, M. I.; Eaves, L.; Morozov, S. V.; *et al.* Field-Effect Tunneling Transistor Based on Vertical Graphene Heterostructures. *Science* **2012**, *335*, 947–950.
32. Soler, J. M.; Artacho, E.; Gale, J. D.; Garcia, A.; Junquera, J.; Ordejon, P.; Sánchez-Portal, D. The SIESTA Method for *Ab Initio* Order-*N* Materials Simulation. *J. Phys.: Condens. Matter* **2002**, *14*, 2745–2779.
33. Dion, M.; Rydberg, H.; Schröder, E.; Langreth, D. C.; Lundqvist, B. I. van der Waals Density Functional for General Geometries. *Phys. Rev. Lett.* **2004**, *92*, 246401–246405.
34. Troullier, N.; Martins, J. L. Efficient Pseudopotentials for Plane-Wave Calculations. *Phys. Rev. B* **1991**, *43*, 1993–2006.
35. Monkhorst, H. J.; Pack, J. D. Special Points for Brillouin-Zone Integrations. *Phys. Rev. B* **1976**, *13*, 5188–5192.
36. Meyer, B.; Vanderbilt, D. *Ab Initio* Study of $BaTiO_3$ and $PbTiO_3$ Surfaces in External Electric Fields. *Phys. Rev. B* **2001**, *63*, 205426–205436.
37. Junquera, J.; Cohen, M. H.; Rabe, K. M. Nanoscale Smoothing and the Analysis of Interfacial Charge and Dipolar Densities. *J. Phys.: Condens. Matter* **2007**, *19*, 213203–213237.
38. Grunner, G. ; Dressel, M. *Electrodynamics of Solids: Optical Properties of Electrons in Matter*; Cambridge University Press: Cambridge, UK, 2012.